Paper No. 938. (quote when citing this article)
Eleventh World Conference on Earthquake Engineering
ISBN: 0 08 042822 3

A STUDY ON SURFACE RESPONSE ANALYSIS OF DIPPING LAYER CONSIDERING EFFECTS OF DIFFRACTED WAVE

T. NISHIKAWA

Department of Architecture, Faculty of Engineering, Tokyo Metropolitan University
1-1, Minami-osawa, Hachioji-shi, Tokyo 192-03, Japan.

T. SEKI
Technical Research Institute, Obayashi Corporation
4-640, Shimokiyoto, Kiyose-shi, Tokyo 204, Japan

ABSTRACT

An approximate method, which is taking the effect of the diffracted waves into account, is presented for the surface ground motion of dipping layer. It is based on the ray theory. This method considers the wave component which propagates along the surface from the edge of a dipping layer as the diffracted wave. Frequency responses and time domain results are presented for different property constants and incident angles. Comparison of results with the boundary element method show very good agreement with low computational cost and without upper frequency limit. The simulation analysis for the ground motions on the heavy disaster belt in the Kobe city by the 1995 Hyogoken-nambu earthquake was conducted using this method and the disaster phenomenon was explained well.

KEYWORDS

Ray theory; diffracted wave; boundary element method; dipping layer; 1995 Hyogoken-nambu earthquake,

INTRODUCTION

The results of investigation on the damage by the 1976 Fliuli earthquake and the 1995 Hyogoken-nambu Earthquake have revealed that serious damage were concentrated in the area where there is a gradual decrease in the thickness of alluvium on the slope of a mountain. It is necessary to investigate the effect of topographic irregular soil on surface response. Many numerical techniques were applied to the study of the seismic behavior of alluvial valleys (Trifunac *et al.*, 1971, Bard and Bouchon, 1980, Sanchez-Sesma *et al.*, 1983). However, in many practical cases computations may become very expensive, if the seismic response is desired for a wide range of frequency. Ray theory (Ishii *et al.*, 1970 ; Sanchez-Sesma *et al.*, 1988) is a powerful method to solve above mentioned problem. The approximate method, based on the ray theory, to calculate the surface response of dipping layer has been proposed (Sanchez-Sesma *et al.*, 1987). An approximate ray was introduced to consider an elastic boundary and different incident angles of an incoming plane wave(Sanchez-Sesma *et al.*, 1988). But they neglected the diffracted wave to choose a special dip angles.

In this paper, an approximate method, which is taking the effect of the diffracted waves into account, is

presented for the surface ground motion of dipping layer. The surface response analyses of the dipping layer and the simulation analysis for the ground motions on the heavy disaster belt by the 1995 Hyogoken-nambu earthquake are conducted using this extended method.

METHODS

The analytical model is assumed to be the dipping layer as shown in Fig. 1. The approximate method to calculate the surface response of dipping layer was proposed (Sanchez-Sesma *et al.*, 1988). In their study, if the dipping angles (θ_d) select the form of $\pi / 2N$,where $N = 3,5,7,\cdots$., there is no diffraction. We extend this method to consider the refracted angle(ϕ) when the incident wave transmits the rock to the deposit (Seki and Nishikawa, 1993). In this case , there is diffraction. The surface response at an arbitrary point can be written as

$$\frac{U}{U_0} = \sum_{j=0}^{M} \sum_{n=0}^{j} \varepsilon_{M-n} \cdot exp\left\{-i \cdot \left(w \cdot H / V_s\right) \cdot \cos\theta_j / \cos\phi\right\} \cdot a_{jn} \prod_{ij} \cdot exp\left(-i \cdot w \cdot S_{ij} / V_s\right) \tag{1}$$

where

$$\theta_j = (N - 2j - 1)\pi / 2N \tag{2}$$

$$S_{jk} = H \cdot \left(\cos\theta_j - \cos\theta_n\right) / \cos\phi + \left|X\right| \cdot \cos\theta'_n + \left|X\right| \cdot \sin\theta'_n \cdot \tan\phi \tag{3}$$

$$\prod_{ij} = \prod_{k=0}^{n} \left(A_k\right) = A_0 \cdot A_1 \cdot A_2 \cdots A_n, \quad S_{jn} \le 0 \tag{4}$$

where $M = (N - 1) / 2, \theta' = \theta_j + \phi, \phi$:refracted angle, U_0: amplitude of incident wave, H: analytical region, a_{jn}:amplitude of refracted wave emitted from point A, ω :circular frequency, V_s:shear velocity, A_k: reflection coefficient, ε_m: Neumann factor (= 1,if m = 0; = 2 if m ≥ 1), X :horizontal coordinate.

NUMERICAL EXAMPLES

Propagation Characteristics of Diffracted Waves

To illustrate the wave motion in the dipping layer, the boundary element method was applied. Fig. 2. displays ground motion for incidence of elastic wave with incident angle $\alpha = 32°$ and dipping angle $\theta_d = 30°$ and properties η $(= V_{sr} \cdot \rho_{sr} / V_s \cdot \rho_{sr}) = 2.0$. In this case, amplitude discontinuity surface lies in the location of the dotted line. Input signal, period $t_p = 1.0$ sec, is a half wave length of sin wave, where t / t_p is dimensionless time. In this figure, incident wave (①) transmitted from the inclined bedrock are shown at $t / t_p = 2.5$ and three types of wave, incident wave (①), reflection wave(②) and diffracted wave(③) , are shown at $t / t_p = 2.5$. As seen from this example, the diffracted wave propagates like a two-dimensional wave in the dipping layer. Next, to illustrate the performance of present method, the amplitudes of the surface displacement obtained from the ray theory (Ishii *et al.*, 1970) and the boundary element method which can be consider the diffraction in the deposit were compared. The incident time signal is a Ricker-type pulse given by

$$f(t) = \frac{\sqrt{\pi}}{2}\left(b^2 - 0.5\right) \cdot exp\left(-b^2\right) \tag{5}$$

where $b = \pi \cdot (t - t_s) / t_p, t_p$:characteristic period of the pulse and $t_s / t_p = 3.0$. The computation were done with the Fast Fourier transform algorithm for $t_p = 1.0$ sec. Fig. 3. illustrates the time history responses. In the

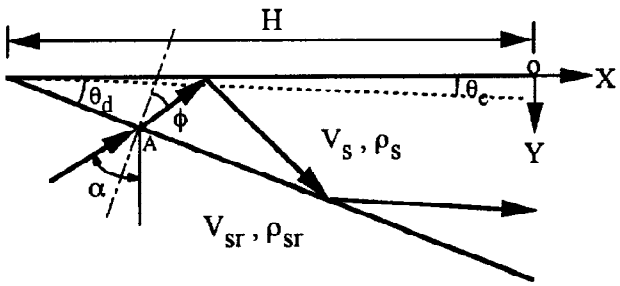

Fig. 1. Analytical model of dipping layer,incident angle α, dipping angle θ_d

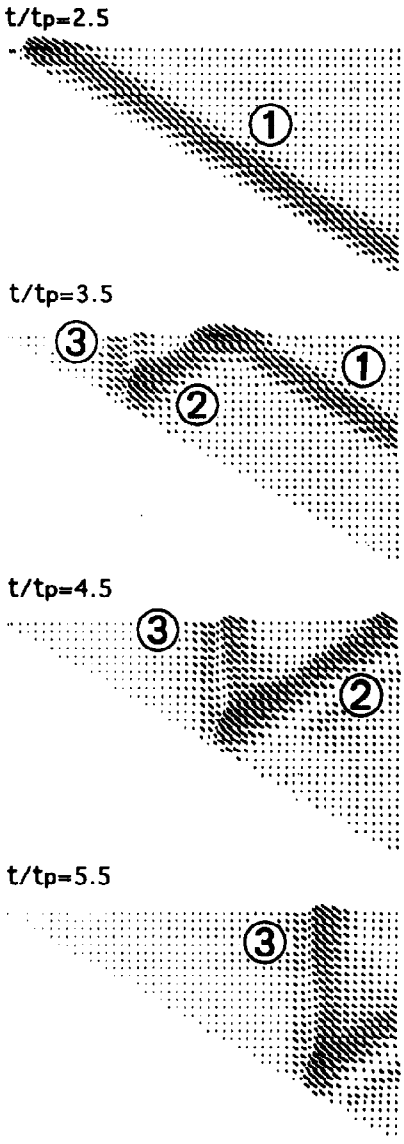

Fig. 2. Variation of ground motion amplitude in the dipping layer. The amplitude of the antiplane motion is given by the length of the oblique segment. The incoming waves are a half wave length of sin waves, incident angle 30° . Impedance ratio η=3.
① = incident wave, ② = reflection wave from the free surface, ③ = diffracted wave generated from the edge.

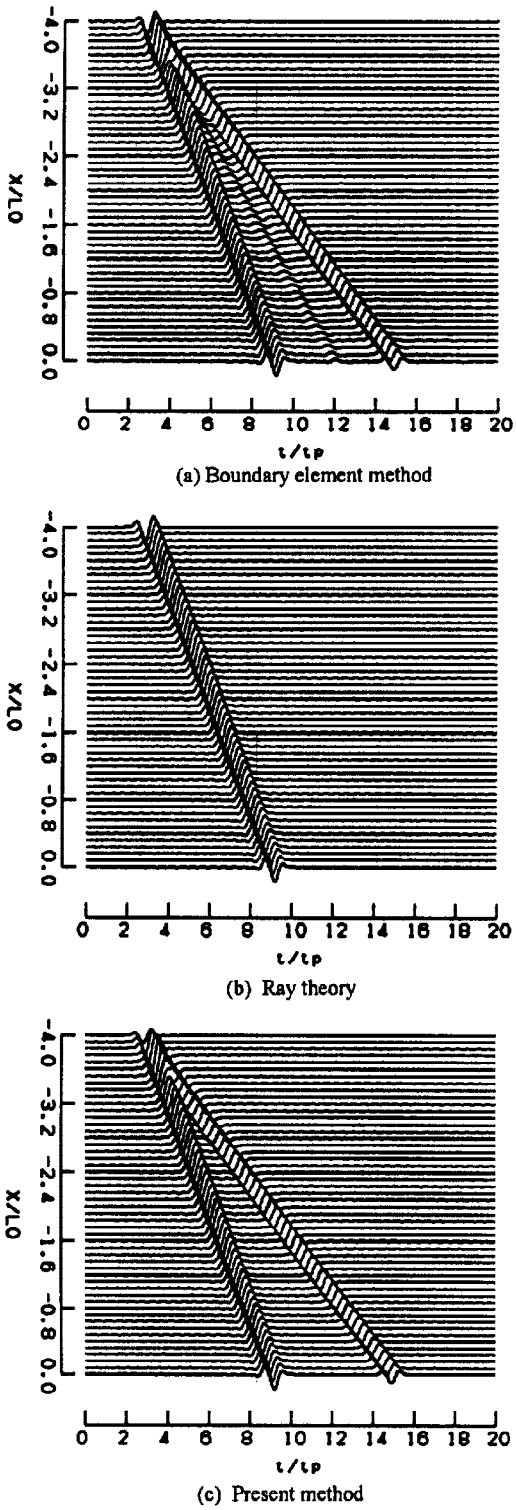

Fig. 3. Synthetic seismograms for the dipping layer, excited by a plane SH wave. The horizontal and vertical axes are dimensionless (t/t_p) and (X/L_o), respectively. L_o is the wave length of incident wave.The synthetic traces by boundary element method, ray theory and present method are compared.

top and bottom of this figures, the time histories of the boundary element method and that of the present method are shown. The middle of this figure shows obtained from the time history of the ray theory. First phase ,which is a common phenomenon, shows the incident wave transmitted from the bedrock and second phase shows the diffracted wave propagated along the surface from the edge. This phase can't be seen in the result from the ray theory because of the ray theory neglect the effect of the diffracted wave.

Relation between Amplitude Discontinuity and Amplitude of the Diffracted Waves

From previous work (Ishii *et al.*, 1970), a discontinuity of the displacement is given by

$$B_0 \cdot \left(\prod_{n=1}^{L} B_n \right) \cdot exp(-ikr) \tag{6}$$

where B_0: amplitude of incident wave, B_1 :refraction coefficient, B_n : reflection coefficients, k :wave number. On the other hand, in case of $j = n = M$ and $\phi = 0$, the last term of the equation (1) can be written as

$$\frac{U}{U_0} = a_{MM} \prod_{ij} A_k \cdot exp\left(-i \cdot w \cdot (H + X) / V_s \right) \tag{7}$$

Then, the amplitudes at the edge obtained from the equations (6) and (7) were compared. In Fig. 4., the displacement amplitudes are displayed for incident harmonic waves with incident angel $\alpha = 0^\circ$ and 30°,respectively, and impedance ratio $\eta\ (= V_{sr} \cdot \rho_{sr} / V_s \cdot \rho_{sr}) = 2$ and 3. In these figures, the displacement amplitudes calculated from the equation (7) agree with the amplitudes discontinuity. Accordingly, the amplitude of the wave component which is expressed equation (7) is equal to the amplitude discontinuity at the dip edge.

The effect of Diffracted Waves on Frequency Responses

To make clear the effect of the diffracted waves on the frequency responses, numerical computation were conducted, in which angles of inclination, physical properties of the soil, and the angle of incident wave were the parameters. The frequency responses with the results of the boundary element method and the ray theory were compared. In Fig. 5. and 6., the frequency response functions are displayed for the incident angle $\alpha = 0^\circ$ and 30°,respectively, upon the dipping layer with dipping angle of 30°,18° and 10° and impedance ratio $\eta = 3$. In these figures, AD presents the amplitude discontinuity and θ_c presents the measured angle from the free surface to the discontinuity surface. The results of this present method are good agreement with the results of the boundary element method rather than those of the ray theory, especially in the lower frequency range. But in the case of the amplitude discontinuity(AD) is small as shown in Fig. 5.(c), there's a little difference between the present method and the ray theory.

Application to The 1995 Hyogoken-Nambu Earthquake

On January 17,1995 Hyogoken-nambu earthquake struck the Kobe City, Hyogo prefecture in the Kansai area of Japan. One of the characteristics of damage is that the narrow heavy disaster area existed, in which almost of structures were suffered heavily damage like collapse, extending form east-northeast to west-southwest across the Kobe city as shown in Fig. 9. To investigate the reason why the damages were concentrated on such that, the simulation analysis were conducted applying the present method. Analytical models were separated into two models, surface structural model and deep structural model, as shown in Fig. 7. Structural cross-section of the profile along N-S through Kobe Univ. were constructed after the result of seismic reflection survey and velocity structures (Iwata *et al.*, 1955). Two steps analyses were conducted. For the first step, the surface motions on the upper Osaka group as the rock outcrop motion using the deep structural model were evaluated. In this case, the deep stratified structure was modeled by a single deposit as shown in Fig. 7(b). and soil properties were evaluated by weighed mean by each layer thickness in Table 2. Fig. 8. shows a schematic representation of the site response to input motion. The input motion **A** is acceleration

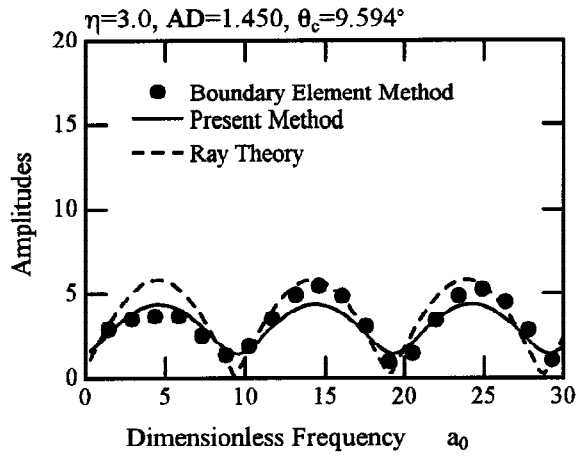

(a) θ_d=30°

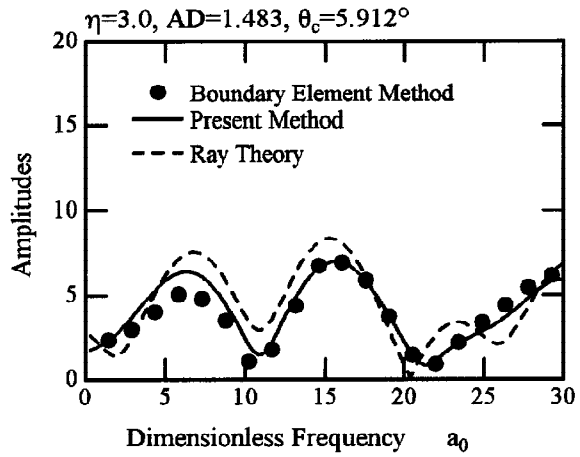

(b) θ_d=18°

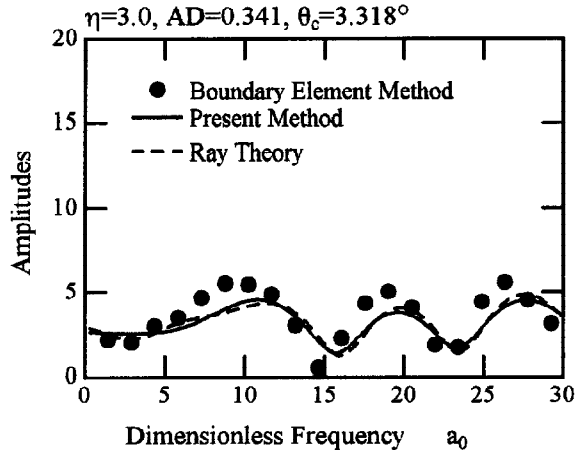

(c) θ_d=10°

Fig. 5. Transfer functions evaluated on the free surface of the model shown in Fig. 1. The horizontal axis is dimensionless frequency a_o, $a_o=\omega|H+X|/V_s$. Solid line shows the present method. Black circle and dotted line correspond to the ones obtained with the boundary element method and ray theory, respectively. Incident angel α=0° .

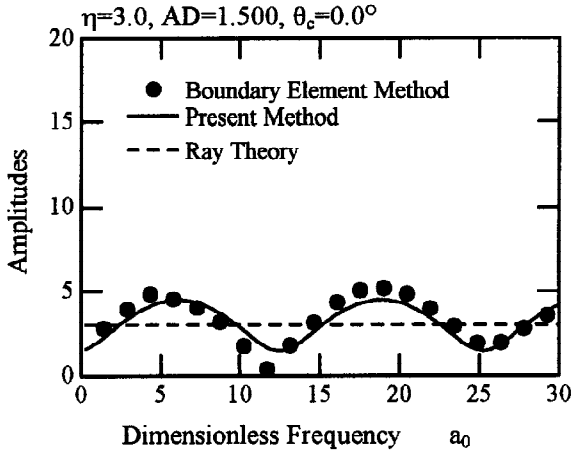

(a) θ_d=30°

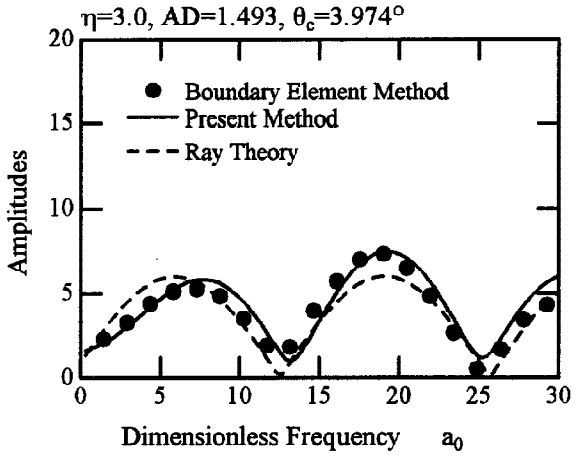

(b) θ_d=18°

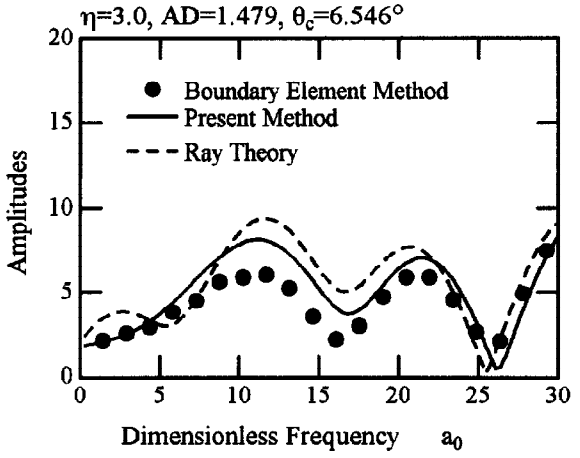

(c) θ_d=10°

Fig. 6. Transfer functions evaluated on the free surface of the model shown in Fig. 1. The horizontal axis is dimensionless frequency a_o. $a_o=\omega|H+X|/V_s$. Solid line shows the present method. Black circle and dotted line correspond to the ones obtained with the boundary element method and ray theory, respectively. Incident angle α=30° .

record, the E-W component, at Kobe Univ. The surface motion, calculated by the 1-D theory, is represented as **C**. The diffracted wave **B**, calculated by the present method, generates from the edge and propagates along the surface laterally. Finally, the resulting surface motion is **D(=B+C)** in Fig. 8. For the second step, non-linear response analyses were conducted using the surface structural model and the surface motion **D** at each points. In this case, the surface deposits were composed of alluvium layer and upper pleistocene layer. Each property was shown in Table 2. and non-linear behavior were introduced by the linear-equivalent method. Fig. 10. shows the relation curves strain-dependent damping factor h and shear modulus G, respectively (Kurimoto *et al.*, 1995). Fig. 11. shows the distribution of maximum acceleration along N-S section. In this figure, dotted line shows rock outcrop motion at the upper part of Osaka group and solid line shows ground surface one. From this figure, maximum acceleration are amplified between Hankyu Line and Route 43 especially and decreased gradually towards sea side. Therefore, the distribution of maximum acceleration is affected to not only the amplification of the surface deposit but also the deep stratified topography. Fig. 12. shows the collapse ratio of buildings and houses along the microseisms observation line in Fig. 9 (Ono *et al.*, 1995). The severer damages were distributed 1.5～2.0 km wide from the JR line in the north to Route 43 in the south. By comparison with Fig. 11. and Fig. 12., the distribution of maximum acceleration along analytical line in Fig. 9. coincided with that of the collapse ratio. Therefore, the heavy disaster belt is caused by focusing effects between the wave passed through the bedrock of the mountain side and the multiple reflection wave in the surface layer.

CONCLUSION

The concluding remarks obtained from the analytical study on the surface response of the dipping layer and the simulation analysis for the ground motions on the heavy disaster belt caused by the 1995 Hyogoken-nambu earthquake are as follow,: (1) The present method is able to take the effect of the diffracted wave into account approximately. (2) Numerical solutions of the present method show good agreement with those of the more rigorous method(boundary element method). (3) This method is suited to study for the surface response of the dipping layer with low cost and without upper frequency limit. (4) The cause of the narrow heavy disaster belt arose from the 1995 Hyogoken-nambu earthquake is the focusing effects between the wave passed through the bedrock of the mountain side and the multiple reflection wave in the surface layer.

ACKNOWLEDGMENTS

We thank the Committee of Earthquake Observation and Research in the Kansai Area for providing us with the acceleration records.

REFERENCES

Ishii, H. and R. M. Elise (1970). Multiple reflection of plane *SH* waves by a dipping layer. *Bull. Seism. Soc. Am., 60,* 15-28.

Iwata, T., K. Hatayama, K. Kawase, K. Irikura. and K. Mastunami (1995). Array observation of aftershocks of the 1995 Hyogoken-nambu earthquake at Higashinada ward, Kobe City. *Journal of Natural Disaster Science, 16,*41-48.

Bard, P.-Y. and M. Bouchon (1980). The seismic response of sediment-filled valleys. Part I. The case of incident *SH* waves. *Bull. Seism. Soc. Am., 70,* 1263-1286.

Kurimoto, O. and T. Fujimori (1995). Analytical method for nonlinear response of soil-structure system. *Proc. of the 4th Structure-Soil Interaction symposium,* 85-92. (in Japanese)

Ono, Y, Ishikawa, K. and S. Mizoguchi (1995). Damage ratio of structures by the 1995 Hyogoken-nambu earthquake. *Proc. of the 50th ann. conf. of the JSCE, 1-(B),* 948-949. (in Japanese)

Sanches-Sesma, F. J. (1983). Diffraction of elastic waves by three-dimensional surface irregularities. *Bull. Seism. Soc. Am., 73, 1621-1636.*

Sanches-Sesma, F. J., F. J. Chavez-Garcia, and M.A. Bravo(1988). Seismic response of a class of alluvial valleys for incident SH waves. *Bull. Seism. Soc. Am., 78,* 83-95.

Seki, T., and T. Nishikawa (1993). Surface response analysis of a dipping layer by ray theory considering effect of diffracted waves. *J. Struct. Constr. Engng, AIJ, 452,* 21-30. (in Japanese)

Trifunac, M.D. (1971). Surface motion of a semi-cylindrical alluvial valley for incident planes *SH* waves. *Bull. Seism. Soc. Am., 61, 1755-1770.*

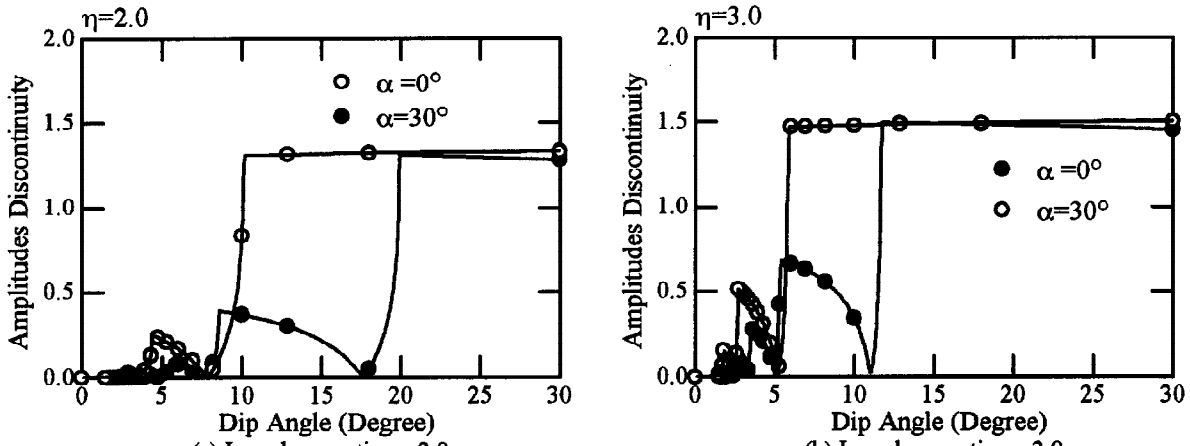

(a) Impedance ratio η=2.0 (b) Impedance ratio η=3.0

Fig. 4. Comparison between displacement amplitude derived from the equation (6) and (7)

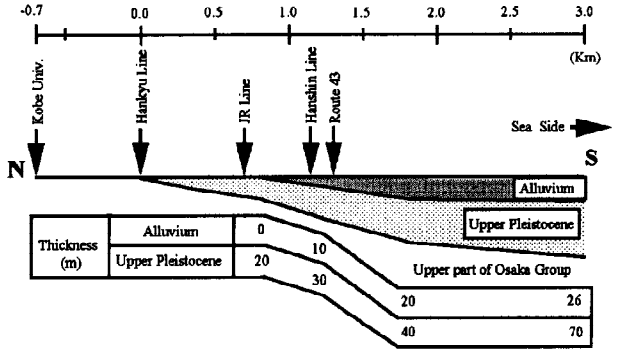

(a) Surface structural cross-section along N-S

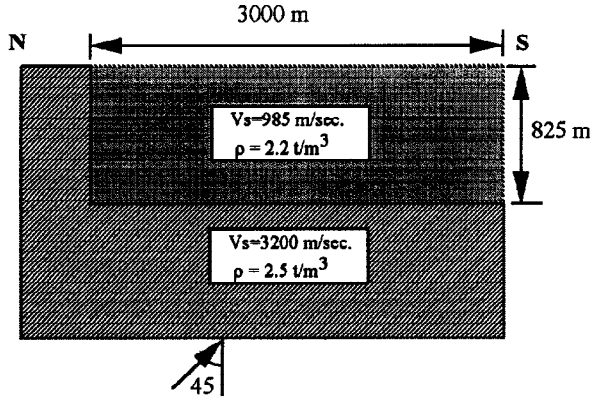

(b) Deep structural cross-section along N-S

Fig. 7. Structural model of cross-section along N-S through Kobe Univ.

Table 1. Stratified structure models for rock site
(after Iwata *et al.*, 1995)

Top Depth (m)	Vs (m/sec)	ρ (t/m³)	Stratigraphic Division
0	1300	2.2	Osaka Group
100	1800	2.4	
550	3200	2.5	

Table 2. Stratified structure models for soil site
(after Iwata *et al.*, 1995)

Top Depth (m)	Vs (m/sec)	ρ (t/m³)	Stratigraphic Division
7	200	1.6	Alluvium
20	300	1.8	Upper Pleistocene
75	500	2.1	Osaka Group
500	1500	2.2	
900	2850	2.3	
1000	3200	2.5	

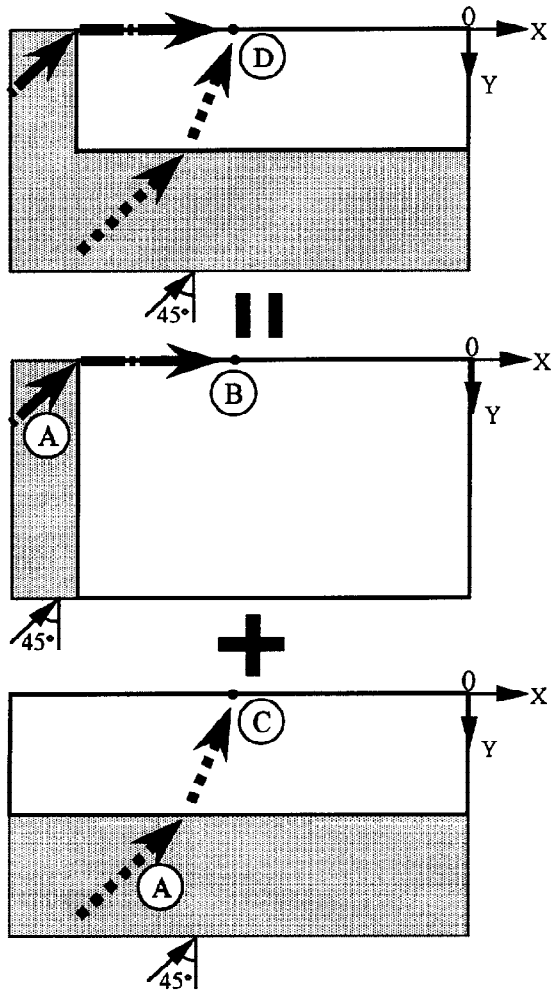

Fig. 8. Schematic representation of the site response to input motion. A=input motion ; B=amplified input motion due to low impedance surface layer; C=diffracted wave generates from the basin edge; D=resulting surface motion due to the amplifiled input motion and the diffracted waves; i.e., D=B+C

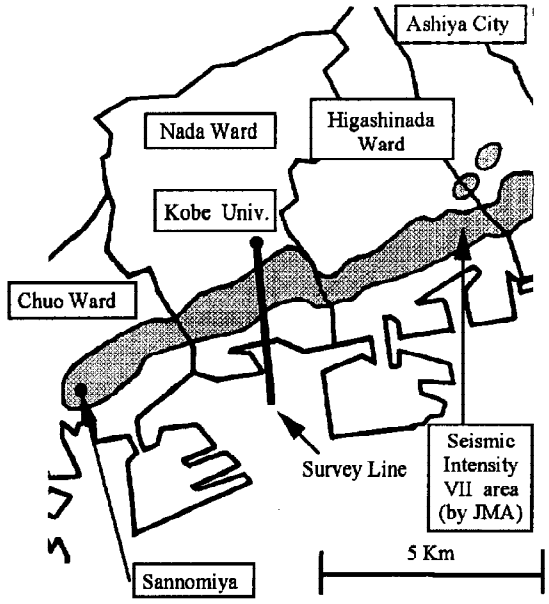

Fig. 9. Location of Survey Line

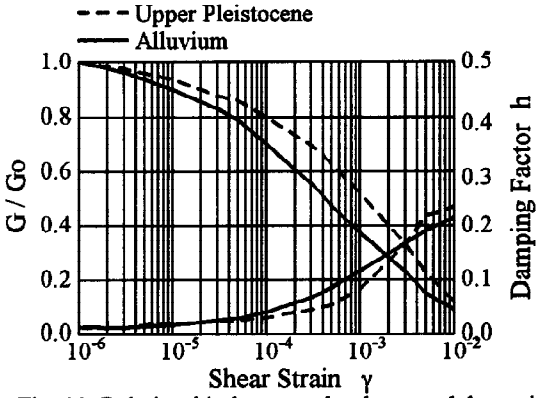

Fig. 10. Relationship between the shear modulus ratio G/G_0 ,damping factor (h) and shear strain γ. Solid line shows Alluvium and dotted line shows Upper Pleistocene. (after Kurimoto et al., 1995)

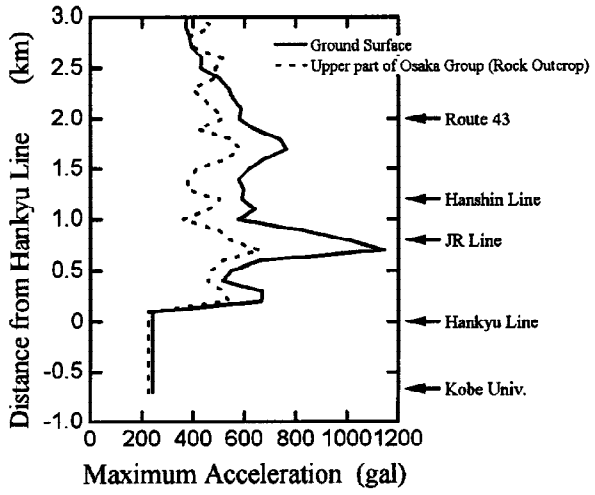

Fig. 11. Distribution of the maximum acceleration

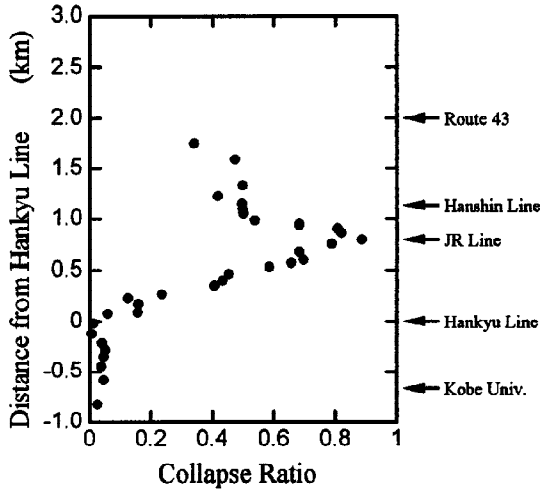

Fig. 12. Collapse ratio of structures along the survey line in Fig. 9. (after Ono et al., 1995)